Magnetoresistive Sensors for Surface Scanning

D.C. Leitão[1], J. Borme[2], A. Orozco[3], S. Cardoso[1,4], and P.P. Freitas[1,4]

[1] INESC-MN and IN, Rua Alves Redol 9, 1000-029 Lisboa, Portugal
dleitao@inesc-mn.pt
[2] INL – International Iberian Nanotechnology Laboratory,
Av. Mestre José Veiga, 4715-31 Braga, Portugal
[3] Neocera, Beltsville, MD, USA
orozco@neocera.com
[4] Instituto Superior Tecnico (IST), Av. Rovisco Pais, 1000-029 Lisboa, Portugal

Abstract. This chapter provides an overview on several techniques used for surface imaging, including SQUIDs, Hall-effect sensors, Giant magneto-impedance sensors, and magnetoresistive (MR) sensors. Among all magnetic field sensors, only SQUIDs and MR devices have the potential to localize buried and non-visual field sources (such as defects in integrated circuits or magnetic field sources in biological environments. In particular, we describe how MR sensors have been used with advantage for integrated circuit (IC) mapping, with resolution below 500 nm and sensitivity to detect currents as low as 50 nA and have been used for many applications requiring low magnetic field detection. Challenges and experimental considerations on integration of MR sensors on a commercial analysis tool are provided here. Examples obtained with real devices demonstrate how Scanning Magnetic Microscopy has become an established failure analysis technique for visualizing current paths in microelectronic devices.

1 Introduction

In recent years has become essential to ensure the reliability, integrity and safety of systems in industry (nuclear, petrochemical, gas) and transport (aeronautics, railway, automotive) sectors. The detection of generation, propagation and failure of a defect in metallic parts is highly desirable, enabling a significant reduction of maintenance costs and consequently improving profit and productivity.

Non destructive testing (NDT) meets this challenge gathering methods to provide information on the health of a structure without impairing its future usefulness. Currently, conventional NDT techniques rely on eddy current (EC) inspection, ultrasonic, and acoustic emission. EC inspection is widespread, ensuring subjacent or surface-breaking flaws detection. EC-NDT works by inducing electrical currents in the structure under test with an electromagnetic field, and thus cracks within the structure distort the EC flow enabling its detection. Nevertheless, EC NDT using traditional inductive sensors has shown difficulty in locating hidden buried defects, low spatial resolution and slow speed of inspection.

Nowadays, the EC inspection method is undergoing a rapid change to answer industry specifications in terms of product quality and cost saving, focusing on the

C. Reig et al.: *Giant Magnetoresistance (GMR) Sensors*, SSMI 6, pp. 275–299.
DOI: 10.1007/978-3-642-37172-1_11 © Springer-Verlag Berlin Heidelberg 2013

detection of small (< 100 μm) and deep flaws (buried under several mm), while decreasing the inspection time.

Among the existent magnetic field detection techniques, only superconducting quantum interference devices (SQUID) [1-3] and magnetoresistive (MR) [4, 5] devices have the potential to localize buried and non-visual field sources. SQUID sensitivity translates to the following in terms of maximum depth and minimum current: 18 μA currents can be detected 1 mm away with a SNR ratio better than 5 [1-3]. Lowering the scanning distance lowers the minimum detectable current: ~ 200 nA can be detected at a distance of 300 μm. Alternatively, increasing the current facilitates detection at a greater distance; for example, 1 mA of current can be detected 54 mm away. However, the extremely high field sensitivity of the SQUID compromises the spatial resolution, and requires complicated apparatus for operation at low temperatures.

These drawbacks motivated the search for alternative NDT methods, such as MR sensors. The excellent spatial resolution of MR sensors has been used with advantage [5]. Their potential for NDT has been addressed in experimental systems namely the detection of cracks on 20 mm thick aluminum [2], to locate and characterize small surface cracks [6], in the evaluation of metal medical implants for invisible cracks [7], inspection of printed circuit boards [8] and detection of hidden corrosion [9]. The detection of very small magnetic fields with high spatial resolution, makes MR sensors ideal for NDT [10, 12, 13] but also for biosensors [11, 13], precision position sensing, document validation [12] and magnetic imaging [14].

Nowadays, the miniaturization levels required in the electronics industry has resulted in complex packaging solutions [15]. Therefore, the difficulty in imaging buried defects or flaws in complicated packaging schemes with multiple stacked devices has increased significantly [Figure 1]. Also, notice that intricate die level analysis is ever more challenging, targeting the accurate detection of buried metallization layers such as 8 to 10 levels down from the chip surface [1, 2, 16]. Currently used non-destructive techniques to detect electrical fails in such complex microelectronic package technologies include Scanning Acoustic Microscopy [16, 17], Scanning SQUID Microscopy [2] and magnetoresistive microscopes [18, 19].

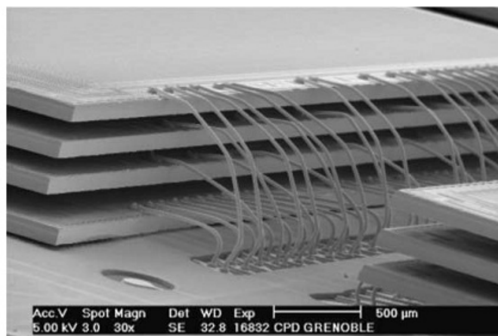

Fig. 1. Example of packaging inspection. Reprinted from Ref. [15] Copyright (2004), with permission from Elsevier.

Next sections will describe briefly some examples where these techniques have been used with advantage for mapping. Finally, section 3.4 will describe how MR sensors have been used for this purpose at an industrial level.

2 Imaging Sensors Devices: Overview

2.1 Flux Sensors

2.1.1 SQUIDs

A scanning superconducting quantum interference device (SQUID) incorporates a superconducting loop containing one or two Josephson junctions. The Josephson junction consists of a thin insulating layer (or constriction) between two superconductors [20, 21]. Overall, when the superconducting loop is submitted to a change in the applied flux applied, a phase difference across the junction will appear due to flowing currents.

In contrast to Hall probes or MR devices where the field sensitivity is nearly independent of the sensing area, in SQUIDs magnetic field sensitivity scales with $1/a^2$ (a is the diameter of the sensing area) [20, 22]. Typically, commercial DC SQUIDs exhibit a magnetic field noise of ~ 10 fT/√Hz [20, 21], still for NDT even small amounts of position noise during scanning can cause significant degradation of the obtained images [23]. Nevertheless, and although SQUIDs provide an extreme sensitivity, they bear the main disadvantage of operating at cryogenic temperatures, at least 77 K for high-T_C superconductors [20].

Several reports using particular designs for highly sensitive scanning SQUID microscope allowed direct observation flux quanta in high-T_C superconducting rings [24, 25]. SQUID microscopy has been used for visualization of magnetic structures at 77 K with a spatial resolution of about 30×10^{-6} m in the vertical component of the magnetic field [28]. Still, recent research on scanning SQUID microscopy focus on room temperature samples, where the main developments target improvements in hardware or software to achieve better spatial resolution [26, 27]. Fong *et al.* were able to image magnetic fields of room-temperature samples with sub-millimeter

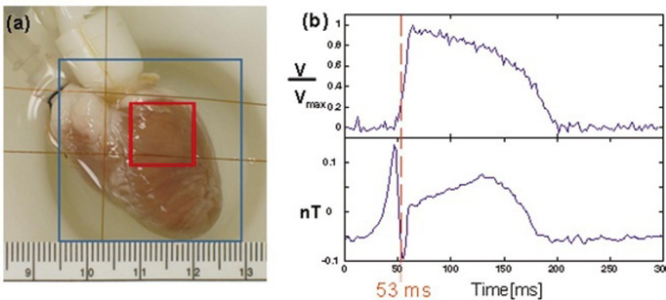

Fig. 2. Time trace of the transmembrane potential and the magnetic field recorded from a rabbit heart (Figure 10 of Ref. [26]). Reprinted with permission from Ref. [26] Copyright (2005), American Institute of Physics.

resolution. Their low-T_C multiloop SQUID sensor provided a field sensitivity of 1.5×10^{-12} T/√Hz, for frequencies above 100 Hz. Figure 2 displays action currents in cardiac tissue imaged by such device. The authors reported field sensitivities on the order of 180×10^{-15} T/√Hz for an optimized 1 mm multiloop SQUID sensor [26].

2.2 Field Sensors

2.2.1 Hall-Effect Sensors

Scanning Hall probe microscopy (SHPM) [29, 30] allows a noninvasive detection of surface magnetic fields. This technique is based on Hall Effect probes, where the changes of the external magnetic field translate into changes in the sensor output voltage [31]. With a theoretical field sensitivity of 2 nT/√Hz [32], SHPM offers a lower sensitivity than SQUID, but allows for nanometer-scale spatial resolution [30], works under variable temperature and variable magnetic field conditions. Figure 3 (left) shows an example of a nano-Hall sensor design [33]. Oral *et al.* described a low-noise SHPM with a magnetic field sensitivity of ~ 2.9×10^{-8} T/√Hz at 77 K and a spatial resolution of ~ 0.85 μm [30]. The same system was successfully operated at room temperature with a magnetic field resolution of ~ 3.8×10^{-6} T/√Hz [30, 34]. In addition, Howells *et al.* showed a high-resolution imaging of a magnetic media at 77 K with a SHPM system displaying a magnetic field sensitivity of 30×10^{-9} T/√Hz and spatial resolution of 0.8 μm [Figure 3(right)] [35].

Chang *et al.* introduced a hybrid Hall/STM microscope which provided a magnetic field sensitivity of ~ 10^{-5} T and a spatial resolution ~ 0.35 μm [36], whilst an optimized planar Hall effect magnetic sensor exhibited a field detection level down to 10^{-9} T [37].

Recently, nanometric Hall sensors with dimensions of ~ 50 nm [Figure 3 (left)] were incorporated into a room temperature SHPM exhibiting an optimum magnetic field sensitivity of 8.0×10^{-5} T/√Hz [33]; quantification of the spatial resolution was lacking. Although electron-beam lithography allows one to prepare sensors with lateral sizes down to the nanoscale range, effective lateral resolution of such a scanning sensor is limited by sensor-sample distance. When the sample is near the end of a measuring tip, its tilting can displace the sensor by hundreds of nanometers, being this the limiting factor of the resolution [38]. However, careful design of the sensor in recent systems claimed a minimum detection size of 80 nm [39].

SHPM systems can be built by attaching a suitable sensor to a commercial table-top AFM [40]. But many SHPM systems are developed to image superconducting materials and must work at cryogenic temperatures [42]. Several authors worked to overcome the small scan range of cooled piezoelectric crystals, either by using stepping motors effectively increasing the range to the centimeter scale [43-45] or by keeping piezoelectric scanner at room temperature while the sample is cooled [41]. Also, in order to reduce the infrastructure needed to operate the systems, others integrated a Stirling cycle refrigeration system allowing the operation at 35 K without the need for cryogenic fluids [46].

Most SHPM systems actually measure the component of the magnetic field perpendicular to the plane of the sample. Using three sensors patterned onto a pyramidal-shaped mesa, Fedor *et al.* [47] developed a SHPM system measuring the three components of the magnetic field.

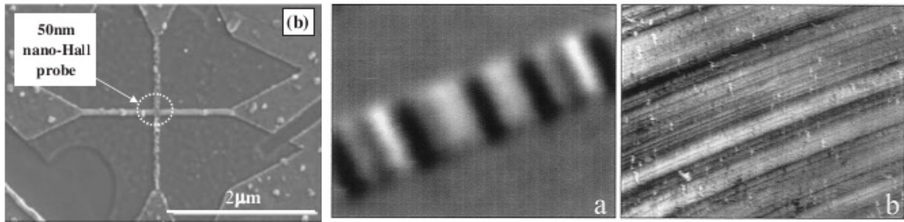

Fig. 3. (left) Nanometric Hall probe (from Ref. [33]). Copyright 2004 The Japan Society of Applied Physics. (middle; rigth) SHPM image at 77 K and simultaneous STM image. Reprinted from Ref. [35], Copyright (1999), with permission from Elsevier.

2.2.2 Giant Magneto Impedance Sensors

When a magnetic field is applied to a soft ferromagnetic conductor which is in turn subjected to a small alternating current (AC), a large change in the AC complex impedance of the conductor is visible [48]. This effect is known as Giant magneto-impedance (GMI) and is the base of GMI sensors, typically made of in metal-based amorphous alloys [48-50]. Although a field sensitivity of a typical GMI sensor can reach a value as high as 500 %/Oe [48, 52], the large size required for the sensing element restricts its spatial resolution [53, 54]. Nevertheless, since the GMI response strongly depends on the composition and shape of the sensor core a double-core GMI sensor based on Co-based amorphous magnetic wires, with reduced size has shown improved sensitivity [55]. The high magnetic field sensitivity of GMI sensors has already proved important in microstructural characterization at close proximity of the samples [56], being also used for detection surface of cracks [53], corrosion defects [56] and embedded flaws [57].

2.2.3 Comparison Table

In table 1 one compares figures of merit of selected sensors discussed above.

3 Magnetoresistive Sensors in Imaging and Scanning Microscopy

The spatial resolution of MR microscopy depends directly on the dimensions of the MR sensor, which in contrast to previously discussed sensors, is readily scalable through fabrication techniques. Furthermore, NDT imaging systems strongly profit from measuring distinctively the 3 components of the magnetic field along distinct directions. Such configuration is easily achieved with engineered MR sensors design. The latter, together with the relatively low cost and ease of implementation of such sensors and their ability of detecting very small magnetic fields give MR devices significant advantages over other magnetic imaging techniques such as SQUID, Hall sensors or Magnetic Force Microscopies.

Table 1. Details and figures of merit concerning NDT sensors, namely SQUID, GMI and Hall probes

Sensor	Particularities	Sensitivity/ Field Detection	Spatial Resolution	Ref.
Scanning Hall Probe Microscopy	AlGaAs/InGaAs/ GaAs	4×10^{-7} T/√Hz @ 300 K	0.08 μm	[39]
	5 μm patterned GaAs/AlGaAs	1×10^{-5} T/√Hz @ 4.2-300 K	5 μm	[44]
	Submicron Hall probe GaAs/AlGaAs	~ 2.9×10^{-8} T/√Hz @ 77 K ~ 3.8×10^{-6} T/√Hz @ 300 K	~0.85 μm	[30] [34]
	hybrid Hall-sensor/STM-positioning	~ 0.36×10^{-4} T/√Hz @ 4.2 K	~0.35 μm	[36]
	Planar Hall effect FeNi on Si(100)	300 V $T^{-1}A^{-1}$ @ 300 K	N/A	[37]
GMI sensors	Amorphous wire based	Up to 500 %/Oe @ 300 K	Low and size dependent	[52]
Scanning SQUID microscopy	high-T_C superconducting	N/A	30 μm (magnetic field vertical component)	[28]
	low-T_C niobium bare	1.5×10^{-12} T/√Hz	80 μm (sensor diameter)	[26]
	low-T_C niobium multiloop	$480 – 180 \times 10^{-15}$ T/√Hz	250 μm - 1 mm (sensor diameter)	[26]

The idea of using MR sensors as element to detect magnetic stray fields stems from the widely implemented hard-disk-heads, typically used to read information from hard disk media. In fact, the first reports concerning scanning MR microscopy used commercial MR record/playback heads as sensing elements which were raster scanned over particular magnetic samples [58-61]. Following these studies, the MR microscope system has been adapted to perform magnetic domain imaging on steel sheets [62] and nondestructive testing of materials [63]. Application of magnetic imaging to other research fields include the detection of defects in metallic plates [64, 65], in aircraft structures [66] and metallic containers used in nuclear power plants [67] showing ability to detect defects embedded 7 mm inside the metal, and land mine buried up to 8 cm inside the ground [68].

In particular, GMR based sensors have been successfully used in EC testing of nonmagnetic metals accurately detecting small surface-breaking cracks [7]. These probes had small dimensions and high sensitivities (220 mV/mT) with resolutions of 10 μT over a broad frequency range. Besides GMR, other types of magnetoresistive sensors are also used for the imaging applications such as anisotropic magnetoresistance (AMR) [69] and tunnel magnetoresistance (TMR) [70], although the first being the most used in current works. Still, AMR effect sensors are actively used in imaging either for scanning MR microscopy [71] or in multichannel scanning systems [72].

3.1 Arrays of Individual MR Sensors

When more than one individual sensor is located on a chip, the additional available information allows imaging and scanning of larger areas, and determining the location of magnetic objects. The use of arrays can provide substantial gains of scanning speed, or even remove the need for scanning and of moving parts altogether. Notice that, scanning over a surface or volume using a single sensor has the advantage of being an uniform measurement, while in arrays of magnetic sensors a dispersion in their properties of magnetic sensors will be reflected in the final result. Also, in the case of the scanning technique one is allowed to choose the spatial resolution by setting appropriate scanning speed and data acquisition rate, whereas an array provides a fixed value where the minimum distance is physically set by the individual sensor size, or by the size of each bridge arrangement of sensors. To compensate for the granularity and enhance the visual output, isolines of interpolated data can be used [73]. On the other hand, scanning systems often show line to line differences, which can be addressed during post-process data by a digital 3x3 low-pass convolution filter [74] or by other functions available in scanning-probe data analysis software. Another possibility to measure distances smaller than those provided by the sensor spacing resorts to the use of a fixed array together with a scanning system, the latter providing small displacements [75].

Due to fabrication reasons, most works use in-line or in-plane sensors. However, sensors can be disposed on a molded shape, allowing field imaging of industrial parts with known shapes [75]. The easiest way to obtain an array of sensors is to arrange discrete commercial sensors. Cano *et al.* [72] used 16 commercials in-line AMR sensors spaced by 5 mm, to scan in one direction over the surface of a magnetized sample with a magnetic field resolution of 0.1 μT. The same authors later used a scanning device equipped with 3 sensors with a smaller measurable field of 10 nT and with the capability to image the three components of the magnetic field by scanning over a surface. Other works extended the scanning method to the measurement of a volume using a three-axis stepper motor system [73]. As usually a MR sensor is sensitive to only one component of the field. However, the use of triple-axis magnetometers provides complementary information which can prove essential when a defect can be clearly evidenced in a specific field component [70].

When discrete sensors are used together, a higher data throughput can be obtained, but at the expense of complex wiring and control electronics. Moreover, and due to its compatibility with CMOS technology, a complete device can incorporate signal

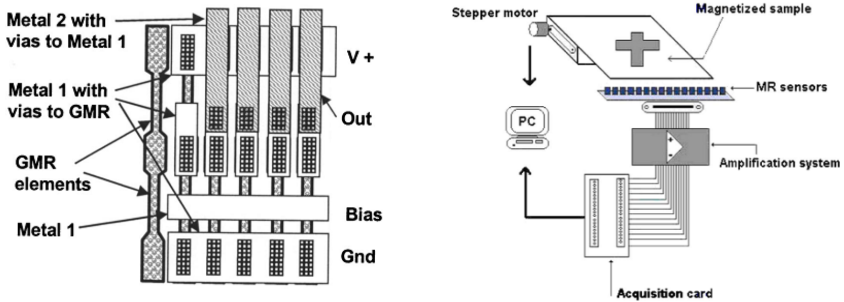

Fig. 4. (left) Example of a 16 element array. Reprinted with permission from Ref. [5]. Copyright (2003), American Institute of Physics. (right) Example of a sensor array measurement set-up. Reprinted with permission from Ref. [72]. Copyright (2005), American Institute of Physics.

conditioning and logic features besides the micrometer-scale MR sensor providing an optimized overall system performance [5]. In fact, large-scale integration of these sensors boosted a strong progress on the materials side, as smaller and denser elements required higher magnetic anisotropy [76]. Furthermore, intense research effort in large MR sensor arrays is devoted to assays [77], with an emphasis in compatibility with spotter technology [78, 79]. Additional works on biomedical applications focus also on simultaneous measurement of several sensors to provide imaging of biological samples or kinetics in solution [80].

3.2 Gradiometer Configuration

In a gradiometer, two magnetic elements are present and the signal measured depends on the difference of the magnetic fields at the two positions. Indeck *et al.* [81] introduced a magnetoresistive gradiometer composed of two MR sensors connected in a Wheatstone bridge, showing a reduction of thermal drift by one order of magnitude. In the case of a single MR sensor connected within a bridge in magnetometer configuration, magnetic shields are commonly used to render particular sensors insensitive. In the case of a gradiometer, these shields are often not required as two active sensors are used. Moreover, pairs of sensors in gradiometers configuration can be arranged in arrays for faster scanning or imaging.

Since two sensors are used for each measurement point, specific geometric considerations have to be taken into account, e.g. while scanning along a defect, the width of one sensor cannot exceed half the size of the smallest defect to be detected [82]. Such configurations can be used in the non-destructive control of metal parts to detect cracks [83] or inclusions of non-magnetic materials [84].

3.3 Cantilever MR Probes

MR sensors either AMR or GMR based, have already been used in scanning MR microscopy integrated in the back side of a cantilever [Figure 5]. In these systems,

the sensor measures the magnetic fields while the cantilever detects the surface morphology [85, 86]. For hybrid AMR cantilever a lateral spatial resolution of a few mm and a field sensitivity of 0.17 mT were reported [85]. Recently, Sahoo *et al.* [87] used the MR sensor to detect the cantilever displacement, instead of the typical optical or piezoelectric detection modes. In this case, one aims to translate the cantilever displacement into a change in the magnetic field sensed by a MR sensor in close proximity. Here, MR sensors offer the advantages of high bandwidth (in excess of 1 MHz), small form factor, straightforward integration and scalability providing a route for high-throughput scanning probe microscope devices. The proposed solutions by Sahoo *et al.* rely on having a micromagnet attached to the end of the moving cantilever and a MR sensor placed at a fixed position relative to the cantilever [Figure 5]. Hence, a change in the cantilever position will induce a change in the magnetic field created by the micromagnet on the sensing layer of the MR probe, thus changing its resistance. Figure 5 (bottom) shows MR scanning probe microscopy contact-mode imaging of a surface using one of the architecture suggested in Ref. [87]. The authors envisaged a resolution of 84 pm achieved over a bandwidth of 1 MHz, overcoming the 200 pm (over 1 MHz) achievable using optical means in state-of-the-art AFMs.

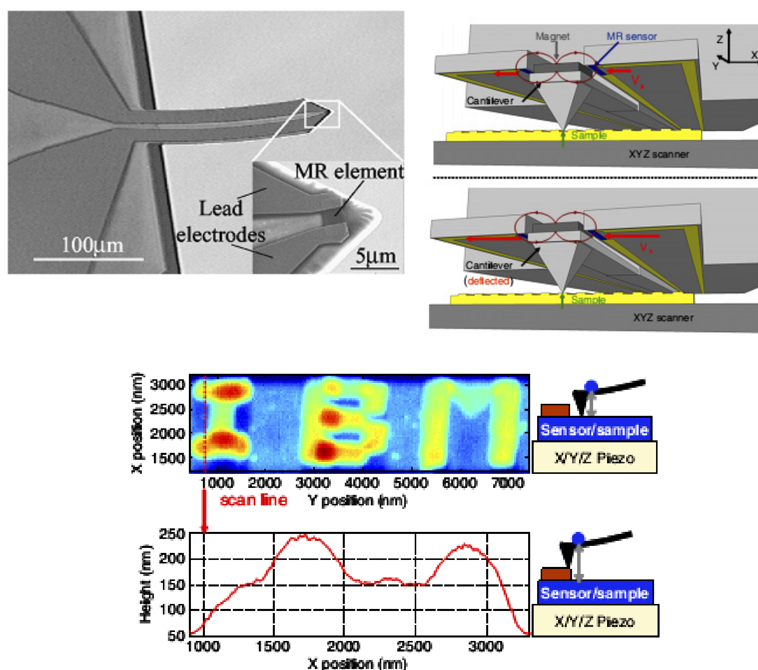

Fig. 5. (top) Examples of hybrid cantilever/MR sensor designs. (top-left) Reprinted with permission from Ref [85]. Copyright (2002), American Institute of Physics. (top-rigth) Reprinted with permission from Ref [87]. Copyright (2011), Institute of Physics (IOP). (bottom) Output of a MR-SPM system operating in contact mode. Reprinted with permission from Ref [87]. Copyright (2011), Institute of Physics (IOP).

3.4 Comparison of MR Sensors

The following table compares the distinct particularities and performance of selected MR based devices for NDT.

Table 2. Details and figures of merit multiple MR sensors

	Particularities and details		Sensitivity	Field Detection	Ref.
Magnetoresistive Sensors	Isolated Sensor Multilayer	conventional	0.04 %/G	N/A	[5]
		low hysteresis	0.07 %/G		
		high sensitivity	0.2 %/G		
	half-bridge Multilayer	conventional	0.2 mV/V/G	20 nV/nT @10 V	
		low hysteresis	0.35 mV/V/G	25 nV/nT @10 V	
		high sensitivity	1.0 mV/V/G	100 nV/nT @10 V	
	TMR	40 % TMR; 1.5 nm Al_2O_3 barrier	30 mV/V/G	3 mV/nT @10 V	[103]
	Phillips KMZ10A (16 channel)	AMR thin film NiFe	0.1 µT	N/A	[72]
	Bridge configuration of 4 barber pole 256 channel;	AMR; Ta/Ru/IrMn/Ru/NiFe/Ta	0.1 mT@ 8 kscans/s.	20 nT/√Hz	[102]
	-	GMR	10 µT	220 mV/mT	[7]
	Hybrid Sensor/ Cantilever	AMR; 40 nm-thick NiFe	0.17 mT	N/A	[85]

4 Magnetoresistive Microscopy for Die Level Fault

Test and Failure Analysis (FA) of integrated circuits (IC) and micro-devices is becoming an increasingly complex science. The ever-shrinking nature of the silicon technology and increased complexity of design and packaging has been making the search of root cause failure a difficult problem. This has forced the industry over the years to search for new techniques and tools to find defects that require increased sub-micron resolution with lower power consumption and more difficult access to circuits and transistors because of increased levels of metallization involved. To complicate things even more, in addition to the miniaturization trend, the need to expand functionality, form factor and real-state management and faster connections have pushed the industry to develop complex 3D package integration. This 3D circuit

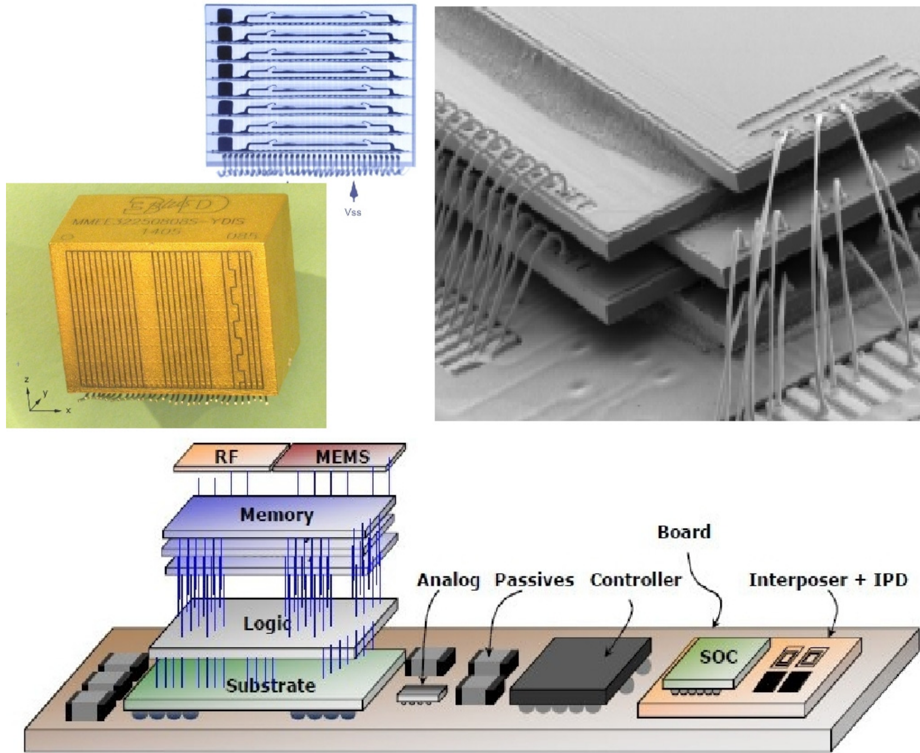

Fig. 6. Several examples of complex packaging

technology includes System-in-Package (SiP), wafer-level packaging, through-Silicon-vias (TSV), stacked-die and flex packages among others that calls for vertical stacking of multiple dies, fully integrated interconnects within Silicon and multiplication of opaque and metal layers, as exemplified in Figure 6.

The presence of buried, non-visual defects has forced scientist and engineers to develop new techniques to locate the failure location and to innovate in existing ones in order to keep pace with the trends and needs of the semiconductor industry and consequently, there is a myriad of acronyms right now for all the different techniques being currently used by the FA community. Complexities of present-day and future designs require use of nondestructive, non-contact fault isolation tools and techniques capable of guiding the FA engineer accurately, reliably, and quickly through multiple layers to the failure location.

Among them, magnetic field imaging, using SQUIDs as the sensing element, was introduced in 1998 [88] as a way to detect short circuit failures in ICs. The principle is very simple: the circuit of interest in the device under test (DUT) is powered up. The current generates a magnetic field around it and this magnetic field is detected by a sensor above the device. The sample is raster scanned and magnetic field is acquired at determined steps providing a magnetic image of the field distribution.

This magnetic field data is typically processed using an standard inversion technique [27, 89] to obtain a current density map of the device. The resulting current map can then be compared to a circuit diagram, an optical or infrared image, or a non-failing part to determine the fault location. In this sense, magnetic field imaging allows the Engineer to "see" what the current is doing in the DUT. Recent advances expanding the bandwidth of operation of SQUID sensors has allowed the localization of open circuit failures by detecting radio-frequency (RF) magnetic fields [1, 90].

The main advantage of magnetic imaging is that is a fully non-destructive, non-invasive, contact-less technique. In addition, magnetic signals generated by the current in the device under test pass unaffected by virtually all materials used in modern packaging technologies. It can thus see through multiple layers of metal, insulator and even multiple dies vertically stacked. All this makes magnetic imaging an excellent technique for Fault Isolation (FI) of defects and it is currently established as a standard technique for isolating shorts, leakages and high resistance defects in packages and die, as well as distinguishing between package-level and die-level defects [2, 16, 92-96].

As SQUIDs operate at cryogenic temperatures (typically at 77 K for high-temperature superconductors), they need to be isolated from the environment by an enclosure under vacuum while the DUT is raster scanned, at room temperature, under the sensor. The presence of the enclosure limits how close to the surface one can scan a sample. Ultimately, resolution is limited by the scanning distance or the sensor size and thus, SQUID imaging resolution is limited to about 25 μm lateral resolution for typical scanning distances and device thicknesses.

In FA, though, resolution is linked to failure localization accuracy, being this a better descriptor of a technique's capability. Failure localization accuracy is defined as the ability to correlate a defect through physical deprocessing results with the signature obtained from the fault isolation tool to meet or exceed some expected resolution. These two terms, lateral resolution and defect localization accuracy are often used to refer to the same concept: how good can a tool or technique physically locate the defect.

Magnetic imaging as applied to FI normally uses the processed current density image to pinpoint the failure location. Because of this, a peak localization technique allows, by use of software, to improve defect localization to about 3 μm.

Using magnetic imaging for FA imposes demanding restrictions on the type of sensor that can be used. There are three main requirements that are linked: need of high resolution, high magnetic field sensitivity (and thus, low noise figures) and the geometry of the sensor itself.

As stated before, SQUID sensors provide very high sensitivity and resolution in the few microns, making them ideal for packaged devices. They also provide coarse localization for die-level fault isolation. They lack, however, the submicron resolution required for die-level analysis. MR-based sensors on the other hand can be manufactured in small sizes, they operate at room temperature and noise figures have improved substantially in the recent years to provide enough sensitivity to be usable for FA [3, 12, 97-101]. Furthermore, they can be fabricated in a tapered-tip shape which allows for getting close to wirebonds or probe needles in front-side scanning situations as well as scanning in milled-out cavities [12].

4.1 Sensitivity

The key figure of merit for sensitivity in FA is minimum current detection. The reason is that the own nature of the defect can make it very sensitive to applied current or voltage and in some situations, too large voltage or current can result in the destruction of the defect or "healing" of the device. Besides that, different devices have different requirements in terms of limiting voltage and current. In general, FA Engineers tend to be on the safe side and restrict the current levels to < 1 mA with 20 mA to be typically considered too high. In addition, the need to locate defect leakage currents which can be as low as 20 nA imposes additional restrictions to the sensor sensitivity.

On the other hand, for magnetic imaging, the key figure is magnetic field sensitivity. There are two components to determine the magnetic field sensitivity when it comes to magnetic field scanning for FA: the intrinsic noise figure of the magnetic sensor used and the overall signal-to-noise ratio (S/N) for the image acquisition equipment. We will consider the second to be optimized for the application and identical for different type of sensors allowing us to just focus on intrinsic sensor noise figures.

The link between magnetic field sensitivity and minimum detectable current is obviously the distance from the current source to the sensor. For fixed scanning distance (that is, sensor-to-current distance), the sensor with better magnetic field sensitivity (lower noise figure) will allow for the lowest detectable current, making it the most desirable.

MR sensors used for magnetic field imaging in FA are typically based on a spin-valve (SV) or a magnetic tunnel junction (MTJ) device. Although MTJ sensors have larger response as compared to SV, the comparatively simple design, low voltage noise, high yield, and robust physical characteristics of SV sensors make them attractive for initial development and integration in commercial magnetic field microscopes [12, 101].

For practical imaging applications, the field noise of the sensor provides the best figure of merit for a sensitivity comparison and can be measured the same way for all sensors, including SQUIDs. Field noise measurements represent the minimum field that can be measured at a given frequency above the noise floor of the sensor and associated electronics. Figure 7 shows noise data for a SQUID, MTJ, commercial SV (hard-drive head), and an optimized SV sensor for failure analysis.

The SV and MTJ sensors only reach a white noise response beyond the upper end of this frequency range, so there is a steady improvement as a function of frequency. At 10 kHz, the MTJ sensor has a noise level of approximately 1 $nT/\sqrt{Hz}$. The optimized SV sensors have a noise level of approximately 6 $nT/\sqrt{Hz}$, 2 orders of magnitude better than SV hard-drive heads, which have a noise level of 900 $nT/\sqrt{Hz}$ at 10 kHz. These noise figure improvements directly translate into improvements in minimum current detectability in magnetic field imaging. For identical image S/N, the amount of current required scales directly with the noise level of the sensor. For example, an image of a circuit carrying 2 μArms imaged with an optimized SV sensor would require, under identical configuration and conditions, approximately 300 μArms to obtain the same quality image with a SV hard-drive sensor.

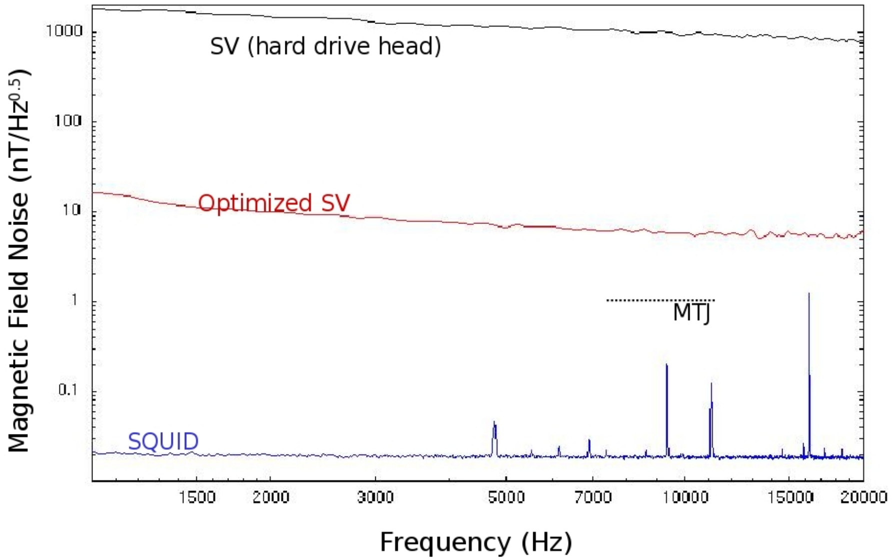

Fig. 7. Magnetic field noise as a function of frequency for SQUIDs, SV hard-drive heads, optimized SV sensors, and MTJs. Optimized SV sensors show 2 orders of improvement over conventional MR hard-drive heads.

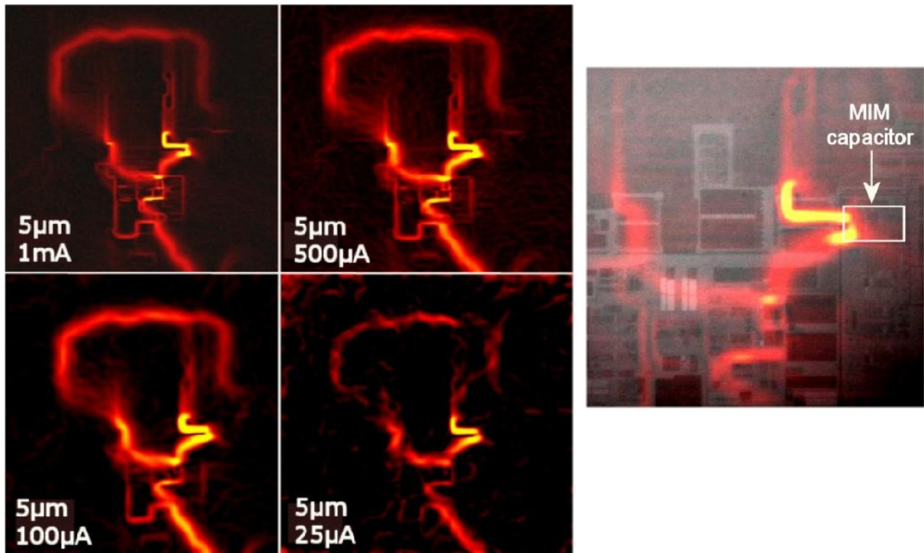

Fig. 8. (left) Current density image from backside scanning decreasing the current for a 5 μm thinned down die. (right) Zoom in detail of the current path at the defect MIM capacitor. The current image is overlaid with the infra-red (IR) image of the die. Images courtesy of M. Hechtl, Infineon.

The effect of current into the resulting images acquired with SV MR sensors has been widely studied. An excellent example was presented in the paper by M. Hechtl [100] and can be summarized in Figure 8(left) showing current density images from identical scans from the back side of a flip-chip mounted IC. A 5 µm-thick thinned down die was scanned using a commercial magnetic field imaging system. Identical scans were acquired except for varying the current for each scan from 1 mA to 25 µA. The impact of reducing the current on the sharpness, resolution and clarity of the images is evident.

Figure 8(right) shows the actual defect location, a defective MIM capacitor that was shorted. Two things are worth noticing: first, the SV sensor has enough sensitivity to locate the defect when applying just 25 µA of current to the device, as seen by the presence of the bright current paths produced by the short. The intensity of the current seen on the zoomed image on the MIM capacitor actually reveal that even lower current could have been used and the defect could have still been detected. Although details on the circuit parts that carry less current are vanishing progressively as the current decreases, just 1 mA of current is enough to reveal many details of the circuitry. Second, sensitivity and resolution are linked together. The lower the current, the less details of the circuit can be obtained.

The same author also did a study on how distance impacts current detectability and resolution. Figure 9(left) shows current density images for the same device scanned from the back side. In this case, the die was thinned down from 200 µm to 5 µm while all other conditions were kept identical. Obviously, the thinner the die, the closer the sensor-to-current distance.

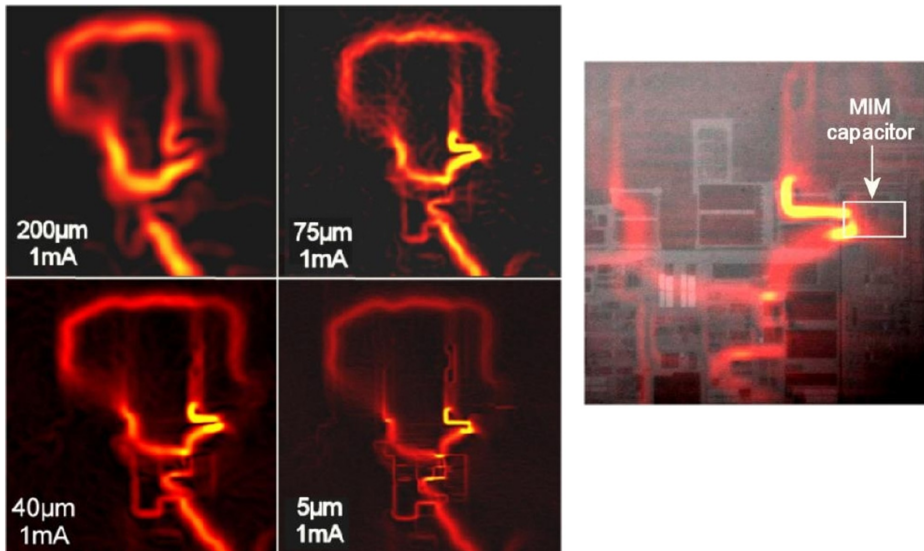

Fig. 9. (left) Current density image detected by the SV sensor at a current of 1 mA for different die thickness. (right) Zoom in detail of the current path at the defect MIM capacitor. The current image overlaid with the infra-red (IR) image of the die. Images courtesy of M. Hechtl, Infineon.

A large portion of the path structure can be identified by comparison with the top metallization layout of the interposer and only some short metal line of the bottom interposer layer is involved in the current path shown, appearing as blurred, as it is farthest away from the scanning sensor. At about 75 µm, the rectangular shape of the on-die current paths are distinct enough, a clear sign of resolution improvement.

It is remarkable that the image reveals not only on-die currents but also interposed current paths that are further away.

4.2 Resolution and Sensor Geometry

The resolution, d, for a sensor is proportional to the sensor-to-current distance, z, and the lateral dimensions, w, of the sensing area as $d \sim (4\ z^2 + w^2)^{0.5}$. MR sensors, with active sensing dimension along the scanning direction smaller than 50 nm, are thus capable of sub-micron resolution if allowed to scan in close proximity with the circuit under investigation. In principle, this makes them ideal candidates for front-side scanning providing nano-scale resolution but for actual device scanning, equally important to sensitivity and resolution is probe tip geometry. The reason for this is that real life device scanning requires electrical connection to the circuit that is done by either using probe needles, or, in the case of packaged devices, wirebonding to the package interconnect. Furthermore, for backside or packaged devices with no direct access to the circuitry, sometimes it is necessary to mill out a cavity on a previously identified coarse region that allows closer proximity to achieve higher resolution. These cavities are normally small in dimensions as the laser milling or focused-ion-beam (FIB) time required to machine them are very costly.

To illustrate this problem, let's consider, for example a typical MR hard drive sensor. These sensors are mounted on a rigid cantilever and have a footprint of roughly 1.5 mm × 1 mm. The size and the mounting geometry can make access to the die in a decapsulated chip difficult at best.

Figure 10 shows a hard-drive MR sensor probe positioned on a 1 cm × 1 cm die. In addition to the size of the sensor substrate itself, the cantilever supporting the sensor, as noticed on the left inset and right insets, extends well beyond the sensor block, thus risking contact with and damage to wirebonds or needles (Figure 10, right inset). They are also difficult or impossible to operate on very small dies.

SV MR sensors for FA has been designed with a body that tapers to a point, in a pencil-like shape with a footprint less than 50 µm × 50 µm. This allows easy access into etched packages, milled out cavities and close proximity (about 5 µm) to wirebonds and probe needles. Figure 11(left) shows a SV MR sensor scanning in a cavity (500 mm × 500 mm and 250 mm deep) of a small die while the image on the right illustrates the capability of the optimized MR sensors to scan in close proximity to wirebonds on a packaged die.

There is an advantage of using a dual sensor approach, like a SQUID/MR combination. The SQUID sensor can do coarse localization of the defect on thick packaged devices. This allows to determine if the problem is in the package, interconnect or die. If the failure location is found on the die, it is relatively easy to

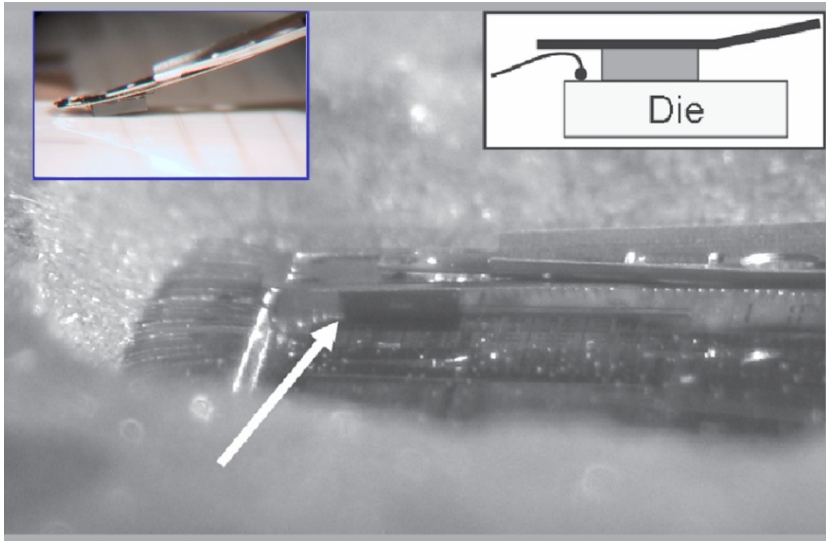

Fig. 10. Conventional MR hard-drive sensor on a die surface, with an illustrated inset. An arrow points to the sensor body mounted under the cantilever. The cantilever supporting the sensor protrudes on all sides, limiting access to the edges of the die.

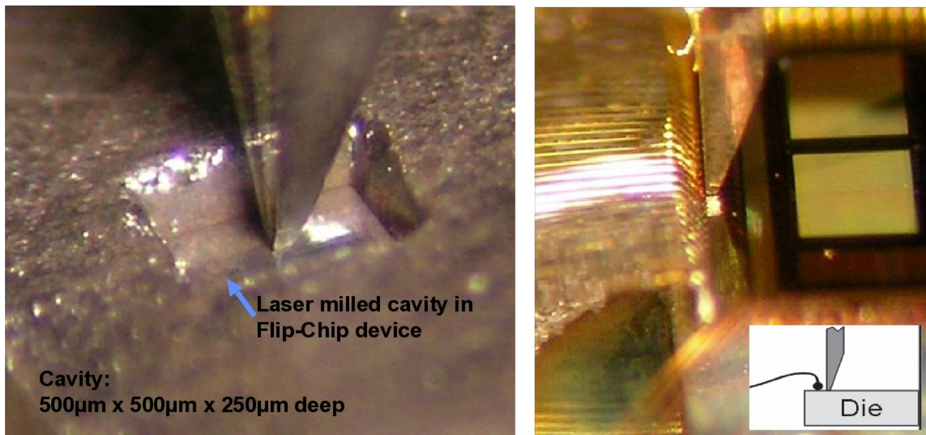

Fig. 11. (left) Local thinning through laser milling provides an opportunity to get closer to an area of interest for high resolution scanning. The SV MR sensor is shown in a cavity that is 500 µm × 500 µm and 250 µm deep. (right) SV MR sensor on a die surface, with an illustrated inset. A high-aspect-ratio tip provides easy access to the die and no restrictions for approaching wirebonds or probe needles.

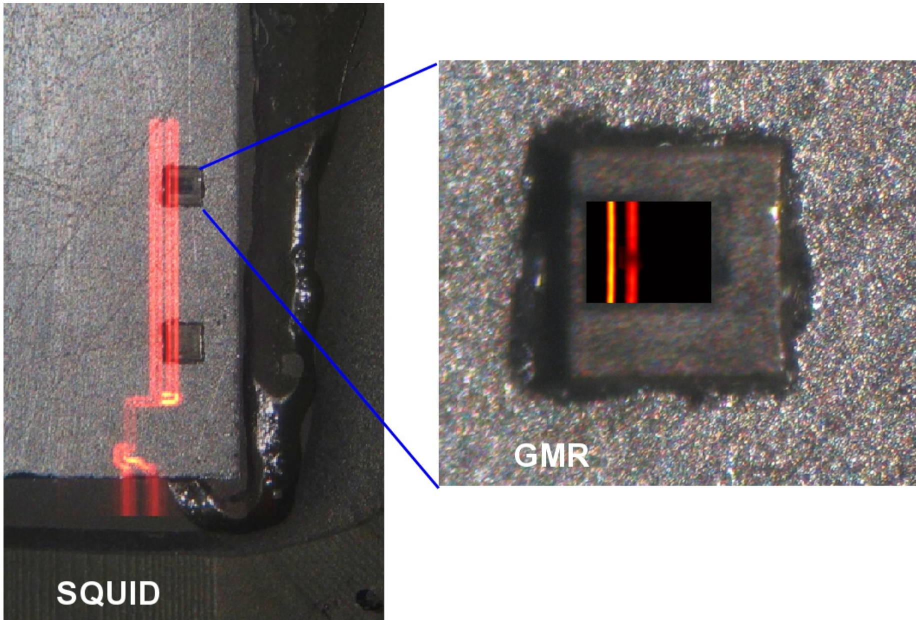

Fig. 12. (left) Current density image of a flip-chip device acquired with SQUID at > 250 mm scanning distance. Current density image is overlaid on optical image. Two FIB milled-out pockets are visible. (right) Current density image inside the cavity (same as shown on Figure 11) acquired with SV MR sensor. Additional details can be seen including a change in level of the current path on the right current path.

partially remove material (like thinning down the die or etching a cavity) to allow the MR sensor to provide the high resolution location of the defect. This is illustrated in Figure 12 where a flip-chip device was first scanned using a SQUID for global current localization [Figure 12(left)]. Two pockets were milled-out using FIB to allow the SV MR sensor tip to go in close proximity and provide better resolution and details [Figure 12(right)]. It can be noticed the difference in metal trace width of the two current lines and also a decrease in current level in the right current path.

The best resolution MR sensors can provide is when having direct access to the circuit, like is the case for front-side accessible devices (exposed die, wafer) as there is only a very thin (few hundreds of nm) passivation layer between the active metal circuit and the sensor. As an example of nano-scale resolution that can be achieved with MR sensor, Figure 13 shows current density images from SV scans of a die serpentine process monitor with 250 nm lines and 400 nm spacing. The two insets show zoom-in current density images of specific areas overlaid on scanning electron microscope (SEM) images to show how the current density matches perfectly the geometry of the metal traces as well as the spacing.

As discussed, there is a trade-off between sensitivity and resolution. The combined use of SQUID/MR sensors is the best way to optimize the data acquired by the system. A magnetic field microscope designed for FA should allow seamless scanning

under one sensor or the other and under an optical camera for physical registration of locations. In this manner, all three images—optical, SQUID, and MR—are registered to each other. This permits easy selection of a region of interest (ROI) to re-scan with higher resolution or to move from the coarse, more sensitive SQUID sensor to the nanoscale-resolution-capable MR sensor. Experience has shown that a coarse scan with the SQUID reveals enough details about the current in the device for initial FI. In a quick and effortless manner, it facilitates identification of ROIs and isolation of defective components (for example, package, die, interconnect level, a particular die in a stacked-die configuration, etc.). With this information, the engineer can select an ROI and increase resolution of the image or even switch to the MR to improve defect localization. Thinning of the die, decapsulation, or other minor sample preparation may be desirable at some point to make it possible for the MR sensor to scan closer to the circuit in the ROI and achieve maximum resolution.

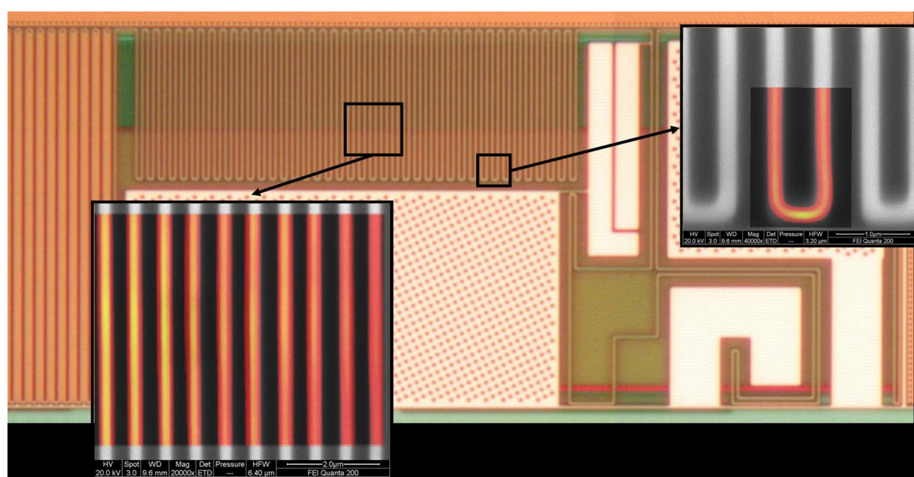

Fig. 13. Nanoscale-resolution current-density image overlaid on the optical image, using the MR sensor, of a test serpentine structure on a wafer. Metal trace width is 250 nm, while the spacing is 400 nm. Higher-resolution images in the insets were overlaid on scanning electron microscopy images.

5 Conclusion

Non destructive testing (NDT) resorting to magnetic imaging is a valuable a non-invasive and non-contact technique to detect either surface or deeply-buried defects in a wide range of structures and devices. In particular using magnetoresistive (MR) sensors for NDT has attracted a considerable attention in recent years as it fulfills the sensitivity and resolution requirements to localize buried and non-visual defects, in particular for complex package integration. Compared to the widely used SQUID devices for NDT, MR sensors have the advantage of being relatively low cost and of

easier implementation. In this chapter, we have shown how MR sensors were successfully used in Scanning Magnetic Microscopy as a failure analysis tool to map current paths in microelectronic devices at an industrial level.

References

[1] Dias, R., Skoglund, L., Wang, Z., Smith, D.: Integration of SQUID Microscopy into FA Flow. In: Proc. 27th Int. Symp. Test. and Failure Analysis (ISTFA), pp. 77–81 (2001)

[2] Pacheco, M., Wang, Z.: Scanning SQUID Microscopy for New Package Technologies. In: Proc. 30th Int. Symp. Test. and Failure Analysis (ISTFA), pp. 67–72 (2004)

[3] Felt, F., Knauss, L., Gilbertson, A., Orozco, A.: Istfa Proc. 33rd Int. Symp. Test. and Failure Analysis, pp. 197–205 (2007)

[4] Ikeda, S., Miura, K., Yamamoto, H., Mizunuma, K., Gan, H.D., Endo, M., Kana, S., Hayakawa, J., Matsukura, F., Ohno, H.: Nat. Materials 9, 721 (2010)

[5] Smith, C.H., Schneider, R.W., Pohm, A.V.: High-resolution giant magnetoresistance on-chip arrays for magnetic imaging. J. Appl. Phys. 93, 6864 (2003)

[6] Sikora, R., Chady, T., Gratkowski, S., Komorowski, M., Stawicki, K.: Eddy Current Testing of Thick Aluminum Plates with Hidden Cracks. In: AIP Conference Proceedings, vol. 657, p. 427 (2003)

[7] Dogaru, T., Smith, S.T.: Giant magnetoresistance-based eddy-current sensor. IEEE Trans. Magn. 37, 3831 (2001)

[8] Dalichaouch, Y., Singsass, A.L., Putris, F., Perry, A.R., Czipott, P.V.: Low frequency electromagnetic technique for nondestructive evaluation. In: Proc. SPIE, vol. 3994, pp. 2–9 (2000)

[9] Crepel, O., Poirier, P., Descamps, P., Desplats, R., Perdu, P., Haller, G., Firiti, A.: Magnetic Microscopy for IC Failure Analysis: Comparative Case Studies using SQUID, GMR and MTJ systems. Microelectronics Reliability 44, 1559 (2004)

[10] Bajjuri, S., Hoffman, J., Siddoju, A., Meyendorf, N.: Development of GMR eddy current sensors for high temperature applications and imaging of corrosion in thick multi-layer structures. In: Proc. SPIE, vol. 5392, pp. 247–255 (2004)

[11] Kataoka, Y., Wakiwaka, H., Shinoura, O.: Proceedings of Sensors 2002, vol. 2, p. 65. IEEE, Piscataway (2002)

[12] Woods, S.I., Orozco, A., Knauss, L.A.: Advances in Magnetic Current Imaging for Die-Level Fault Isolation. Electr. Device Failure Analysis 8(4), 26–30 (2006)

[13] Martins, V.C., Cardoso, F.A., Germano, J., Cardoso, S., Sousa, L., Piedade, M., Freitas, P.P., Fonseca, L.P.: Femtomolar limit of detection with a magnetoresistive biochip. Biosen. Bioelect. 24, 2690–2695 (2009)

[14] Smith, C., Schneider, B.: Sens. Mag. 18, 11 (2001)

[15] Tee, T.Y., Zhong, Z.: Board level solder joint reliability analysis and optimization of pyramidal stacked die BGA packages. Microelectronics Reliability 44, 1957–1965 (2004)

[16] Hechtl, M., Steckert, G., Keller, C.: Localization of Electrical Shorts in Dies and Packages Using Magnetic Microscopy and Lock-In-IR Thermography. In: Proc. 13th Int. Symp. Phys. and Failure Analysis of Integr. Circuits (IPFA) (2006)

[17] Martin, P., El Matouat, A., Legendre, S., Colder, A., Descamps, P.: Fast and accurate method for flaws localization in stacked die packages from acoustic microscopy echoes transients. In: IECON 2011 - 37th Annual Conference on IEEE Industrial Electronics Society (2011)

[18] `http://www.neocera.com`

[19] `http://www.micromagnetics.com`

[20] Jenksy, W.G., Sadeghiz, S.S.H., Wikswo Jr., J.P.: SQUIDs for nondestructive evaluation. J. Phys. D: Appl. Phys. 30, 293 (1997)

[21] Krause, H.-J., Kreutzbruck, M.V.: Recent developments in SQUID NDE. Physica C 368, 70–79 (2002)

[22] Kirtley, J.R., Wikswo Jr, J.P.: Scanning Squid Microscopy. Annu. Rev. Mater. Sci. 29, 117–148 (1999)

[23] Lee, S.-Y., Matthews, J., Wellstood, F.C.: Position noise in scanning superconducting quantum interference device microscopy. Appl. Phys. Lett. 84, 5001 (2004)

[24] Kirtley, J.R., Ketchen, M.B., Stawiasz, K.G., Sun, J.Z., Gallagher, W.J., Blanton, S.H., Wind, S.J.: High-resolution scanning SQUID microscope. Appl. Phys. Lett. 66, 1138 (1995)

[25] Tsuei, C.C., Kirtley, J.R., Chi, C.C., Yu-Jahnes, L.S., Gupta, A., Shaw, T., Sun, J.Z., Ketchen, M.B.: Pairing Symmetry and Flux Quantization in a Tricrystal Superconducting Ring of $YBa_2Cu_3O_7$-δ. Phys. Rev. Lett. 73, 593 (1993)

[26] Fong, L.E., Holzer, J.R., McBride, K.K., Lima, E.A., Baudenbacher, F., Radparvar, M.: High-resolution room-temperature sample scanning superconducting quantum interference device microscope configurable for geological and biomagnetic applications. Rev. Sci. Instrum. 76, 053703 (2005)

[27] Chatraphorn, S., Fleet, E.F., Wellstood, F.C., Knauss, L.A., Eiles, T.M.: Scanning SQUID microscopy of integrated circuits. Appl. Phys. Lett. 76, 2304 (2000)

[28] Crankshaw, D.S., Trias, E., Orlando, T.P.: Magnetic Flux Controlled Josephson Array Oscillators. IEEE Transactions on Applied Superconductivity II(I), 1223 (2001)

[29] Davidović, D., Kumar, S., Reich, D.H., Siegel, J., Field, S.B., Tiberio, R.C., Hey, R., Ploog, K.: Phys. Rev. Lett. 76, 815 (1996)

[30] Oral, A., Bending, S.J., Henini, M.: Real-time scanning Hall probe microscopy. Appl. Phys. Lett. 69, 1324 (1996)

[31] Heremans, J.: Solid state magnetic field sensors and applications. J. Phys. D Appl. Phys. 26, 1149–1168 (1993)

[32] Boero, G., Demierre, M., Besse, P.-.A., Popovic, R.S.: Micro-Hall devices: performance, technologies and applications. Sensors and Actuators A: Physical 106(1-3), 314–320 (2003)

[33] Sandhu, A., Kurosawa, K., Dede, M., Oral, A.: 50 nm Hall Sensors for Room Temperature Scanning Hall Probe Microscopy. Japanese Journal of Applied Physics 43(2), 777–778 (2004)

[34] Oral, A., Bending, S.J., Henini, M.: Scanning Hall probe microscopy of superconductors and magnetic materials. J. Vac. Sci. Technol. B14, 1202 (1996)

[35] Howells, G.D., Oral, A., Bending, S.J., Andrews, S.R., Squire, P.T., Rice, P., de Lozanne, A., Bland, J.A.C., Kaya, I., Henini, M.: Scanning Hall probe microscopy of ferromagnetic structures. Journal of Magnetism and Magnetic Materials 196-197, 917–919 (1999)

[36] Chang, A.M., Hallen, H.D., Harriott, L., Hess, H.F., Kao, H.L., Kwo, J., Miller, R.E., Wolfe, R., van der Ziel, J., Chang, T.Y.: Scanning Hall probe microscopy. Appl. Phys. Lett. 61, 1974 (1992)

[37] Nguyen Van Dau, F., Schuhl, A., Childress, J.R., Sussiau, M.: Magnetic sensors for nanotesla detection using planar Hall Effect. Sens. Act. A 53, 256–260 (1996)

[38] Dinner, R.B., Beasley, M.R., Moler, K.A.: Cryogenic scanning Hall-probe microscope with centimeter scan range and submicron resolution. Rev. Sci. Instrum. 76, 103702 (2005)

[39] Pross, A., Crisan, A.I., Bending, S.J., Mosser, V., Konczykowski, M.: Second-generation quantum-well sensors for room-temperature scanning Hall probe microscopy. J. Appl. Phys. 97, 096105 (2005)
[40] Schweinböck, T., Weiss, D., Lipinski, M., Eberl, K.: Scanning Hall probe microscopy with shear force distance control. J. Appl. Phys. 87, 6496 (2000)
[41] Sandhu, A., Masuda, H., Senoguchi, H., Togawa, K.: Nanotechnology 15, S410 (2004)
[42] Kirtley, J.R.: A novel variable temperature scanning nano-Hall probe microscope system for large area magnetic imaging incorporating piezoelectric actuators maintained at room temperature. Rep. Prog. Phys. 73, 126501 (2010)
[43] Kustov, M., Laczkowski, P., Hykel, D., Hasselbach, K., D-Bouchiat, F., O'Brien, D., Kauffmann, P., Grechishkin, R., Givord, D., Reyne, G., Cugat, O., Dempsey, N.M.: Magnetic characterization of micropatterned Nd-Fe-B hard magnetic films using scanning Hall probe microscopy. J. Appl. Phys. 108, 63914 (2010)
[44] Cambel, V., Fedor, J., Gregušová, D., Kováč, P., Hušek, I.: Large-scale high-resolution scanning Hall probe microscope used for MgB2 filament characterization. Supercond. Sci. Technol. 18, 417 (2005)
[45] Perkins, G.K., Bugoslavsky, Y.V., Qi, X., MacManus-Driscoll, J.L., Caplin, A.D.: High field scanning Hall probe imaging of high temperature superconductors. IEEE Trans. Appl. Superc. 11(1), 3186–3189 (2001), doi:10.1109/77.919740
[46] Gregory, J.K., Bending, S.J., Sandhu, A.: A scanning Hall probe microscope for large area magnetic imaging down to cryogenic temperatures. Rev. Sci. Instrum. 73, 3515 (2002)
[47] Fedor, J., Cambel, V., Gregušová, D., Hanzelka, P., Dérer, J., Volko, J.: Scanning vector Hall probe microscope. Rev. Sci. Instrum. 74, 5105 (2003)
[48] Phan, M.-H., Peng, H.-X.: Giant magnetoimpedance materials: fundamentals and applications. Prog. Mater. Sci. 53, 323–420 (2008)
[49] Beach, R.S., Berkowitz, A.E.: Giant magnetic field dependent impedance of amorphous FeCoSiB wire. Appl. Phys. Lett. 64, 3652 (1994)
[50] Panina, L.V., Mohri, K., Bushida, K., Noda, M.: Giant magneto-impedance and magneto-inductive effects in amorphous alloys. J. Appl. Phys. 76, 6198 (1994)
[51] Panina, L.V., Mohri, K.: Magneto-impedance effect in amorphous wires. Appl. Phys. Lett. 65, 1189 (1994)
[52] Ripka, P.: Magnetic sensors and magnetometers. Artech House Publishers (2001)
[53] Goktepe, M., Ege, Y., Bayri, N., Atalay, S.: Non-destructive crack detection using GMI sensor. Phys. Status Solidi (c) 1, 3436–3439 (2004)
[54] Hamia, R., Cordier, C., Saez, S., Dolabdjian, C.: Giant magneto impedance sensor for nondestructive evaluation eddy current system. Sens. Lett. 7, 437–441 (2009)
[55] Tehranchi, M.M., Ranjbaran, M., Eftekhari, H.: A Double core giant magneto-impedance sensors for the inspection of magnetic flux leakage from metal surface cracks. Sensors and Actuators A 170, 55–61 (2011)
[56] Kim, D.J., Park, D.G., Hong, J.H.: Nondestructive evaluation of reactor pressure vessel steels using the giant magnetoimpedance sensor. J. Appl. Phys. 91, 7421–7423 (2002)
[57] Vacher, F., Alves, F., Gilles-Pascaud, C.: Eddy current nondestructive testing with giant magneto-impedance sensor. NDTE Int. 40, 439–442 (2007)
[58] Yamamoto, S.Y., Schultz, S.: Scanning magnetoresistance microscopy. Appl. Phys. Lett. 69, 3263 (1996)
[59] Yamamoto, S.Y., Schultz, S.: Scanning magnetoresistance microscopy (SMRM): Imaging with a MR head. J. Appl. Phys. 81, 4696 (1997)

[60] O'Barr, Lederman, M., Schultz, S.: A scanning microscope using a magnetoresistive head as the sensing element. J. Appl. Phys. 79, 6067 (1996)
[61] Yamamoto, S.Y., Vier, D.C., Schultz, S.: High resolution contact recording and diagnostics with a raster-scanned MR head. IEEE Trans. Magn. 32, 3410 (1996)
[62] So, M.H., Nicholson, P.I., Meydan, T., Moses, A.J.: Non-destructive surface inspection system for steel and other ferromagnetic materials using magneto-resistive sensors. IEEE Trans. Magn. 31, 3370 (1995)
[63] Nicholson, P.I., So, M.H., Meydan, T., Moses, A.J.: J. Magn. Magn. Mater. 160, 162 (1996)
[64] Smith, C.H., Schneider, R.W., Dogaru, T., Smith, S.T.: Eddy-Current Testing with GMR Magnetic Sensor Arrays. In: AIP Conf. Proc., vol. 700, pp. 406–413.
[65] Postolache, O., Ribeiro, A.L., Ramos, H.: Uniform eddy current probe implementation using planar excitation coil and GMR sensor array. In: Proceedings IMEKO TC4 (2011)
[66] Yashan, A., Bisle, W., Meier, T.: Inspection of hidden defects in metal-metal joints of aircraft structures using eddy current technique with GMR sensor array. In: Proc. 9th ECNDT, Berlin (2006)
[67] Vacher, F., Gilles-pascaud, C., Decitre, J.M., Fermon, C., Pannetier, M.: Non destructive testing with GMR magnetic sensor arrays. In: Proc. 9th ECNDT, Berlin (2006)
[68] Vyhnánek, J., Janošek, M., Ripka, P.: AMR gradiometer for mine detection. Sensors and Actuators A 186, 100–104 (2012)
[69] Janosek, M., Vyhnanek, J., Ripka, P.: CW metal detector based on AMR sensor array. Sensors 28-31, 1515–1517 (2011)
[70] Holzl, C.H.P.A., Wiesner, T., Zagar, B.G.: Quality assurance for wire connections used in integrated circuits via magnetic imaging. In: 2012 IEEE International Instrumentation and Measurement Technology Conference (I2MTC) (2012)
[71] Phillips, G.N., Eisenberg, M., Draaisma, E.A., Abelmann, L., Lodder, J.C.: IEEE Transactions on Magnetics 38 (2002)
[72] Cano, M.E., Martínez, J.C., Bernal-Alvarado, J., Sosa, M., Córdova, T.: 16-channel magnetoresistive scanner for magnetic surface imaging. Rev. Sci. Instrum. 76, 086106 (2005)
[73] Tumanski, S., Liszka, A.: The methods and devices for scanning of magnetic fields. Journal of Magnetism and Magnetic Materials 242–245, 1253–1256 (2002)
[74] Cano, M.E., Pacheco, A.H., Cordova, T., Mazon, E.E., Barrera, A.: Superficial magnetic imaging by an xy-scanner of three magnetoresistive channels. Rev. Sci. Instrum. 83, 033705 (2012)
[75] Mook, G., Michel, F., Simonin, J.: Electromagnetic Imaging Using Probe Arrays. Journal of Mechanical Engineering 57(3), 227–236 (2011)
[76] Pohm, A.V., Beech, R.S., Bade, P.A., Chen, E.Y., Daughton, J.M.: Analysis of 0.1 to 0.3 micron wide, ultra dense GMR memory elements. IEEE Trans. Mag. 6(30), 4650–4652 (1994)
[77] Baselt, D.R., Lee, G.U., Natesan, M., Metzger, S.W., Sheehan, P.E., Colton, R.J.: Biosensors & Bioelectronics 13, 731–739 (1998)
[78] Han, S.-J., Xu, L., Yu, H., Wilson, R.J., White, R.L., Pourmand, N., Wang, S.X.: CMOS Integrated DNA Microarray Based on GMR Sensors. In: International Electron Devices Meeting (IEDM 2006) (2006)
[79] Freitas, P.P., Cardoso, F.A., Martins, V.C., Martins, S.A.M., Loureiro, J., Amaral, J., Chaves, R.C., Cardoso, S., Germano, J., Piedade, M.S., Sebastião, A.M., Fonseca, L.F., Pannetier-Lecoeur, M., Fermon, C.: Spintronic platforms for biomedical applications. Lab-on-Chip 12(3), 546–557 (2012)

[80] Gaster, R.S., Xu, L., Han, S.-J., Wilson, R.J., Hall, D.A., Osterfeld, S.J., Yu, H., Wang, S.X.: Quantification of protein interactions and solution transport using high-density GMR sensor arrays. Nature Nanotechnology 6, 314–320 (2011)
[81] Indeck, R.S., Judy, J.H., Iwasaki, S.: A magnetoresistive gradiometer. IEEE Trans. Mag. 6(24), 2617–2619 (1988)
[82] Pelkner, M., Neubauer, A., Reimund, V., Kreutzbruck, M., Schütze, A.: Routes for GMR-Sensor Design in Non-Destructive Testing. Sensors 12(9), 12169–12183 (2012)
[83] Kreutzbruck, M., Neubauer, A., Pelkner, M., Reimund, V.: Adapted GMR Array used in Magnetic Flux Leakage Inspection: 18th World Conference on Nondestructive Testing, Durban, South Africa, April 16-20 (2012)
[84] Kloster, A., Kröning, M., Smorodinsky, J., Ustinov, V.: Linear magnetic stray flux array based on GMR gradiometers. In: Indian Society for Non-Destructive Testing (NDE 2002), ISNT Chapters in Chennai, Kalpakkam & Sriharikota, December 5-7 (2002), http://publica.fraunhofer.de/documents/N-31528.html
[85] Nakamura, M., Kimura, M., Sueoka, K., Mukasa, K.: Scanning magnetoresistance microscopy with a magnetoresistive sensor cantilever. Appl. Phys. Lett. 80, 2713–2715 (2002)
[86] Takezaki, T., Yagisawa, D., Sueoka, K.: Magnetic Field Measurement using Scanning Magnetoresistance Microscope with Spin-Valve Sensor. Jap. J. Appl. Phys. 45, 2251–2254 (2006)
[87] Sahoo, D.R., Sebastian, A., Häberle, W., Pozidis, H., Eleftheriou, E.: Scanning probe microscopy based on magnetoresistive sensing. Nanotechnology 22, 145501 (2011), doi:10.1088/0957-4484/22/14/145501
[88] Knauss, L.A., Frazier, B.M., Christen, H.M., Silliman, S.D., Harshavardhan, K.S., Fleet, E.F., Wellstood, F.C., Mahanpour, M., Ghaemmaghami, A.: Power Shorts from Front and Backside of IC Packages Using Scanning SQUID Microscopy. In: ISTFA 1999: Proceedings of the 25th International Symposium for Testing and Failure Analysis (ASM International), pp. 11–16 (October 1999)
[89] Wikswo, J.P.: The Magnetic Inverse Problem for NDE. In: SQUID Sensors: Fundamentals, Fabrication and Applications, pp. 629–695. Kluwer Academic Publishers, The Netherlands (1996)
[90] Xie, M., Qian, Z., Pacheco, M., Wang, Z., Dias, R., Talanov, V.: Fault Isolation of Open Defects Using Space Domain Reflectometry. In: Proc. 38th Int. Symp. Test. and Failure Analysis, Phoenix, AZ (2012)
[91] Vallett, D.P., Bader, D.A., Talanov, V.V., Gaudestad, J., Gagliolo, N., Orozco, A.: Localization of Dead Open in a Solder Bump by Space Domain Reflectometry. In: Proc. 38th Int. Symp. Test. and Failure Analysis, Phoenix, AZ (2012)
[92] Eng, T.T., Lwin, H.E., Muthu, P., Chin, J.M.: Backside Deprocessing Technique & Its Novel Fault Isolation Application. In: Proc. 12th IPFA, pp. 110–113 (2005)
[93] Woods, S.I., Knauss, L.A., Orozco, A.: Current Imaging Using Magnetic Field Sensors. In: Microelectronics Failure Analysis Desk Reference, 5th edn., pp. 303–311. ASM International (2005)
[94] Orozco, A., et al.: Proc. 29th Int. Symp. Test. and Failure Analysis, Santa Clara, CA, pp. 9–13 (2003)
[95] Orozco, A.: Fault Isolation of Circuit Defects Using Comparative Magnetic Field Imaging, U.S. Patent 7,019,521
[96] Crepel, O., Descamps, P., Poirier, P., Desplants, R., Perdu, P., Firiti, A.: Proc. 30th Int. Symp. Test. and Failure Analysis, Worcester, MA, pp. 29–31 (2004)

[97] Baibich, M.N., Broto, J.M., Fert, A., Nguyen Van Dau, F., Petroff, F., Eitenne, P., Creuzet, G., Friederich, A., Chazelas, J.: Giant Magnetoresistance of (001)Fe/(001)Cr Magnetic Superlattices. Phys. Rev. Lett. 61, 2472 (1988)

[98] Binasch, G., Grünberg, P., Saurenbach, F., Zinn, W.: Enhanced magnetoresistance in layered magnetic structures with antiferromagnetic interlayer exchange. Phys. Rev. B 39, 4828 (1989)

[99] Schrag, B.D., Carter, M.J., Liu, X., Hoftun, J.S., Xiao, G.: Magnetic current imaging with tunnel junction sensors. In: Proc. ISTFA, p. 13 (2006)

[100] Hechtl, M.: Backside GMR Magnetic Microscopy for Flip Chip and Related Microelectronic Devices. IEEE Proceedings of 15th IPFA – 2008, 174–177 (2008)

[101] Orozco, A.: Magnetic Current Imaging in Failure Analysis. Electronic Device Failure Analysis 11, 14–21 (2009)

[102] da Silva, F.C., Halloran, S.T., Kos, A.B., Pappas, D.P.: 256-channel magnetic imaging system. Rev. Sci. Instrum. 79, 013709 (2008)

[103] Tondra, M., Nordman, C.A., Lang, E.H., Reed, D., Jander, A., Akou, S., Daughton, J.M.: Proc. SPIE, vol. 4393, p. 135 (2001)